Therapeutics, Targets, and Chemical Biology

Cancer Research

Evaluation of the Proteasome Inhibitor MLN9708 in Preclinical Models of Human Cancer

Erik Kupperman, Edmund C. Lee, Yueying Cao, Bret Bannerman, Michael Fitzgerald, Allison Berger, Jie Yu, Yu Yang, Paul Hales, Frank Bruzzese, Jane Liu, Jonathan Blank, Khristofer Garcia, Christopher Tsu, Larry Dick, Paul Fleming, Li Yu, Mark Manfredi, Mark Rolfe, and Joe Bolen

Abstract

The proteasome was validated as an oncology target following the clinical success of VELCADE (bortezomib) for injection for the treatment of multiple myeloma and recurring mantle cell lymphoma. Consequently, several groups are pursuing the development of additional small-molecule proteasome inhibitors for both hematologic and solid tumor indications. Here, we describe MLN9708, a selective, orally bioavailable, second-generation proteasome inhibitor that is in phase I clinical development. MLN9708 has a shorter proteasome dissociation half-life and improved pharmacokinetics, pharmacodynamics, and antitumor activity compared with bortezomib. MLN9708 has a larger blood volume distribution at steady state, and analysis of 20S proteasome inhibition and markers of the unfolded protein response confirmed that MLN9708 has greater pharmacodynamic effects in tissues than bortezomib. MLN9708 showed activity in both solid tumor and hematologic preclinical xenograft models, and we found a correlation between greater pharmacodynamic responses and improved antitumor activity. Moreover, antitumor activity was shown via multiple dosing routes, including oral gavage. Taken together, these data support the clinical development of MLN9708 for both hematologic and solid tumor indications. *Cancer Res; 70(5); 1970–80. ©2010 AACR.*

Introduction

The ubiquitin-proteasome system processes the majority of cellular proteins and is the principal manner by which cells regulate protein homeostasis. During normal protein homeostasis, specific proteins are targeted for destruction via the attachment of ubiquitin. These proteasome substrates include misfolded proteins and highly regulated members of critical signaling cascades, including proteins involved in growth control, cell cycle regulation, and apoptosis. Proteasome inhibition results in the stabilization and accumulation of these substrates, leading to the activation of antiproliferative signals, cell cycle disruption, activation of apoptotic pathways, and, ultimately, cell death (1, 2). Rapidly growing malignant cells, already deficient in normal cell cycle checkpoint mechanisms, seem to be highly susceptible to proteasome inhibition (3–6). Therefore, the proteasome emerged as an attractive target for anticancer therapeutics. The success of the first-in-class small-molecule proteasome inhibitor VELCADE (bortezomib) for injection (Millennium Pharmaceuticals, Inc.) validated the proteasome as a therapeutic target for the treatment of human cancer (1, 7–12). VELCADE is approved for the treatment of patients with multiple myeloma and previously treated mantle cell lymphoma (13–21). At present, there are multiple groups in the process of developing small-molecule proteasome inhibitors for various oncology indications. These include both reversible inhibitors, such as CEP-18770, and irreversible inhibitors, such as carfilzomib and NPI-0052. Both CEP-18770 and NPI-0052 are orally active, and all three compounds have shown antitumor activity in preclinical models and are currently in various stages of clinical development (22–30).

The 26S proteasome consists of a 20S multicatalytic core capped on either end with 19S regulatory subunits. The 20S proteasome is a chambered, barrel-like structure containing two heptameric rings made from α subunits and two heptameric rings made from β subunits. The α rings perform capping and gating functions, whereas three of the β subunits (β1, β2, and β5) contain the NH_2-terminal threonines responsible for the different proteasome proteolytic activities. The β1, β2, and β5 subunits are referred to as caspase-like, trypsin-like, and chymotrypsin-like, respectively, because the preferred cleavage site of each subunit is similar to those of other well-known proteases (2, 31–34).

Bortezomib shows time-dependent inhibition of the 20S proteasome by binding to the NH_2-terminal threonine side chain of the catalytic β subunits. Bortezomib exhibits

Authors' Affiliation: Millennium Pharmaceuticals, Inc., Cambridge, Massachusetts

Note: Supplementary data for this article are available at Cancer Research Online (http://cancerres.aacrjournals.org/).

E. Kupperman and E.C. Lee contributed equally to this work.

Corresponding Author: Erik Kupperman, Millennium Pharmaceuticals, Inc., 35 Landsdowne Street, Cambridge, MA 02139. Phone: 617-551-3767; Fax: 617-444-1448; E-mail: erik.kupperman@mpi.com.

doi: 10.1158/0008-5472.CAN-09-2766

inhibitory activity against all three β subunits but preferentially binds to and inhibits the β5 site (35). Although bortezomib has shown clinical efficacy in multiple myeloma and mantle cell lymphoma, to date, it has yet to exhibit strong activity in solid tumor indications, perhaps due to its inability to penetrate into tissues and achieve therapeutically relevant concentrations at those target sites. Therefore, there is a strong rationale for identifying proteasome inhibitors that have different physicochemical or pharmacokinetic properties. Here, we describe the biochemical and preclinical pharmacology data that support the development of MLN9708. MLN9708 is a second-generation small-molecule proteasome inhibitor being developed for the treatment of a broad range of human malignancies. MLN9708 was selected from a large pool of boron-containing proteasome inhibitors based on a physicochemical profile that was distinct from bortezomib. MLN9708 has a shorter 20S proteasome dissociation half-life than bortezomib, which we believe plays an important role in its improved tissue distribution. Direct comparison with bortezomib revealed that MLN9708 has an improved pharmacokinetic and pharmacodynamic profile and shows superior antitumor activity in both solid tumor and hematologic xenograft models, and shows antitumor activity when administered via multiple dosing routes and regimens. MLN9708 is currently being evaluated in multiple phase I clinical studies for both solid- and hematologic-based tumors.

Materials and Methods

Cell Culture

WSU-DLCL2, OCI-Ly7, A375, H460, HCT-116, HT-29, MDA-MB-231, HEK293, and Calu-6 cells were obtained from the American Type Culture Collection and maintained as recommended by the supplier.

In vitro Assays

Kinetic analysis of 20S proteasome inhibition. Kinetic analysis of 20S proteasome inhibition was performed as previously described by Williamson and colleagues (36).

NF-κB-Luc and 4×Ub-Luc cell-based reporter assays. NF-κB-Luc and 4×Ub-Luc cell-based reporter assays were performed as previously described by Williamson and colleagues (36).

Proteasome-Glo IC_{50} and inhibitor washout cell-based assays. Calu-6 cells were cultured in MEM containing 10% fetal bovine serum and 1% penicillin/streptomycin and plated 1 d before the start of the experiment at 10,000 cells per well in a 384-well plate. For IC_{50} determinations, cells were treated with varying concentrations of bortezomib or MLN2238 in DMSO (0.5% final, v/v) for 1 h at 37°C. For reversibility experiments, cells were treated with either 1 μmol/L bortezomib or MLN2238 for 30 min at 37°C and then washed thrice in medium to remove the compounds. Cells were incubated for an additional 4 h at 37°C, after which the medium was removed and replaced with fresh medium. Proteasome activity was assessed by monitoring hydrolysis of the chymotrypsin-like substrate Suc-LLVY-aminoluciferin in the presence of luciferase using the Proteasome-Glo assay reagents according to the manufacturer's instructions (Promega Corp.). Luminescence was measured using a LEADseeker instrument (GE Healthcare Life Sciences).

Pharmacokinetic Studies

Blood and tumor samples were collected before dose and numerous time points after dosing. Each time point represents the average value of three animals. MLN2238 or bortezomib concentrations in blood and plasma samples were determined using a non–good laboratory practice liquid chromatography-tandem mass spectrometry (LC/MS/MS)–based method. MLN2238 or bortezomib was isolated from 50 μL of plasma or blood using a liquid-liquid extraction procedure. Sample (50 μL) was mixed with 50 μL of internal standard solution, 50 μL of 0.5 mol/L HCl, and 500 μL of methyl tertiary butyl ether. The supernatant (300 μL) was then transferred to a clean 96-well plate, evaporated, reconstituted in 100 μL of acetonitrile/water (5:95) containing 0.1% formic acid, and injected onto the LC/MS/MS system for analysis. A reverse-phase gradient method provided sample stacking and separation. Pharmacokinetic analysis of the blood and plasma concentration data was performed using WinNonlin version 5.2 (Pharsight Corp.). Kinetic parameters were estimated using a noncompartmental model using sparse sampling mode (model 201 for plasma and blood). Area under the concentration versus time curve (AUC) and area under the effect versus time curve (AUE) values were calculated using the linear trapezoidal rule.

Pharmacodynamic Studies

Approximately 200 μL of whole blood were collected from each animal and processed for the 20S blood proteasome inhibition assay. Subcutaneous tumors (approximately 600–800 mm^3 in size) were harvested and divided into two or three parts. One was processed for the 20S tissue proteasome inhibition assay, one for Western blot analysis, and one for immunohistochemistry.

Tumor processing for 20S tissue proteasome assays. Frozen samples were pulverized in the Tissue CryoPrep (Covaris) and transferred to glass tubes. After addition of 1 mL of cold tissue lysis buffer [50 mmol/L HEPES (pH 8.0), 1 mmol/L DTT], samples were placed on ice and homogenized as per the manufacturer's instructions using the Covaris E200.

Tumor processing for Western blot assays. Tumors were processed as described above in the Covaris E200. M-PER lysis buffer (Pierce) was supplemented with the following: 1× protease inhibitor cocktail set (Calbiochem), 2 mmol/L sodium orthovanadate (Sigma), 25 mmol/L sodium fluoride, and 25 mmol/L β-glycerophosphate. Cold lysis buffer (300–800 μL) was added to the tumors just before sonication. After sonication, supernatants were transferred to new tubes and protein concentrations were determined.

Western blot analysis. Tumor lysate (50 μg) was loaded onto 4% to 12% Bis-Tris gels (Invitrogen). Proteins were transferred to PVDF-FL membranes (Millipore) using a

semidry transfer apparatus. After transfer and blocking, membranes were incubated with primary antibody overnight at 4°C. Membranes were washed thrice with TBS-Tween 20 (TBST) and incubated with Alexa Fluor 680–labeled goat anti-rabbit immunoglobulin G (Molecular Probes) for 1 h. Membranes were washed five times with TBST and once with TBS while protected from light. Membranes were dried and scanned with the Odyssey Infrared Imaging System (LI-COR Biosciences). The following primary antibodies were used: anti-tubulin (rabbit polyclonal, 1:15,000 dilution; Abcam) and anti–growth arrest DNA damage 34 (GADD34; Proteintech Group, Inc.). Secondary antibody was used at 1:20,000 for tubulin and 1:2,000 for GADD34. Quantitation of Western blot signals was performed with Odyssey software.

20S β5 proteasome tumor and blood assays. 20S β5 proteasome tumor and blood assays were performed as previously described (36–38).

Immunohistochemical studies. Formalin-fixed, paraffin-embedded CWR22 and WSU-DLCL2 xenograft tumor sections (5 μm) were stained with primary antibodies to GADD34, activating transcription factor 3 (ATF3), and cleaved caspase-3 (Proteintech Group, Santa Cruz Biotechnology, and Cell Signaling Technology). The GADD34 and ATF3 antibodies were detected with horseradish peroxidase–labeled secondary antibodies (UltraMap anti-rabbit, Ventana Medical Systems) and incubated with the ChromoMap 3,3′-diaminobenzidine (DAB) kit (Ventana Medical Systems). The cleaved caspase-3 antibody was detected with Alexa Fluor 594–labeled secondary antibody (Invitrogen). Slides were counterstained with hematoxylin for GADD34 and ATF3 assays and 4′,6-diamidino-2-phenylindole for cleaved caspase-3 assay. Images were captured using an Eclipse E800 microscope (Nikon Instruments), 20× objective, and Retiga EXi color digital camera (QImaging). Five fields of view were captured per sample, and images were processed using MetaMorph software (Molecular Devices). Pharmacodynamic marker levels were measured by color thresholding on the DAB or fluorescent signal and measuring area of thresholded signal. Percent positive area was calculated by normalizing with the total area of the field of view.

Animal Care

CB17–severe combined immunodeficient (SCID) and nonobese diabetic (NOD)–SCID mice were housed and maintained in a controlled environment and received food and water *ad libitum*. Veterinary care for the animals was provided in accordance with Millennium Institutional Animal Care and Use Committee.

Efficacy Studies

CWR22 xenografts. Male CB17-SCID mice (Charles River Laboratories), approximately 8 to 11 wk of age, were inoculated s.c. with freshly dissected CWR22 tumor fragments (~20 mg) in the right dorsal flank. Mean tumor volume (MTV) was calculated using the following formula: $0.5 \times (\text{length} \times \text{width}^2)$. When MTV reached approximately 150 to 200 mm^3, animals were randomized into treatment groups ($n = 10$ per group) before dosing. Antitumor activity was determined at the end of the study by calculating the treatment over control (T/C) ratio of their MTVs at the end of the study.

WSU-DLCL2 xenografts. Female CB17-SCID mice, ~6 wk of age, were inoculated s.c. with 4×10^6 WSU-DLCL2 tumor cells suspended in 0.1 mL RPMI 1640 in the right dorsal flank. Animals were randomized, and the MTV and T/C ratio were calculated as described above.

OCI-Ly7-Luc disseminated xenografts. Female NOD-SCID mice, ~9 wk of age, were inoculated i.v. via the tail vein with 1.0×10^6 OCI-Ly7-Luc tumor cells. Mice were randomized into treatment groups ($n = 10$ per group) on day 7 after inoculation. For each imaging session, animals received 150 mg/kg of luciferin (Caliper Life Sciences) via i.p. injection. Animal dorsal and ventral views were imaged to determine total photon flux. Images were captured by the Xenogen IVIS imaging system (Xenogen Corp.), and data were collected with Xenogen Living Image software (Living Image 3.0.2.2). Antitumor activity was determined by calculating the T/C ratio of the mean photon flux measurements at the end of the study. Survival curves were generated using the Kaplan-Meier method.

Statistical Analyses

Efficacy data were analyzed using a linear mixed-effect regression model. Differences among mice were treated as random effects, and a compound symmetry covariance structure was used to model the variability between repeated tumor measurements for each mouse. Treatment comparisons were performed by taking fitted curves from the model to calculate ΔAUCs. The significance of the ΔAUC was assessed using permutation testing. P values of ≤0.05 were considered significant. For the OCI-Ly7-Luc study, differences in total photon flux among mice were compared using one-way ANOVA and pairwise comparisons were adjusted by the Tukey-Kramer method. Survival curves generated using the Kaplan-Meier methods were compared using the log-rank (Mantel-Cox) test and pairwise comparisons were adjusted with the Bonferroni correction.

Results and Discussion

MLN2238 is a selective, potent, and reversible inhibitor of the proteasome. MLN9708 was identified in screens for small-molecule proteasome inhibitors with an improved pharmacologic profile compared with bortezomib (Fig. 1). In preclinical studies, MLN9708 immediately hydrolyzed to MLN2238 (see Supplementary Data), the biologically active form, on exposure to aqueous solutions or plasma. In studies where a solution of MLN9708 was added directly into rat, dog, or human plasma and immediately extracted and analyzed by high-performance liquid chromatography, only MLN2238 could be identified. MLN2238 is an N-capped dipeptidyl leucine boronic acid and preferentially bound to and inhibited the chymotrypsin-like proteolytic (β5) site

of the 20S proteasome with an IC_{50} value of 3.4 nmol/L (K_i of 0.93 nmol/L; Table 1). At higher concentrations, it also inhibited the caspase-like (β1) and trypsin-like (β2) proteolytic sites (IC_{50} of 31 and 3,500 nmol/L, respectively). Although the selectivity and potency of MLN2238 were similar to that of bortezomib, the proteasome binding kinetics for these two molecules are different. Both MLN2238 and bortezomib showed time-dependent reversible proteasome inhibition; however, the proteasome dissociation half-life ($t_{1/2}$) for MLN2238 was determined to be ~6-fold faster than that of bortezomib ($t_{1/2}$ of 18 and 110 minutes, respectively).

MLN2238 is a potent inhibitor of the proteasome in tumor cells. To build on the biochemistry results, a series of cell-based experiments were performed to confirm potent proteasome inhibition in cells. Proteasome inhibition results in the stabilization and accumulation of ubiquitinated proteins, which have been targeted for destruction. This leads to cell cycle disruption, activation of apoptotic pathways, and active cell death (39–43). Initial studies examined the effects of MLN2238 treatment on an exogenous proteasome substrate. MDA-MB-231 cells expressing a 4×Ub-Luc reporter (36) were treated with increasing concentrations of MLN2238 and bortezomib. Both compounds strongly inhibited proteasome activity, resulting in accumulation of the luciferase reporter with similar EC_{50} values (Table 1). The effect of bortezomib and MLN2238 on tumor necrosis factor-α (TNF-α)–induced activation of the NF-κB pathway was also examined (44). Proteasome inhibition prevents the degradation of IκBα, an inhibitor of NF-κB, resulting in a decrease in NF-κB–driven gene expression. HEK293 cells stably expressing a NF-κB-Luc reporter were treated with increasing concentrations of MLN2238 and bortezomib. Both compounds strongly inhibited TNF-α–induced activation of the NF-κB pathway, resulting in similar EC_{50} values (Table 1).

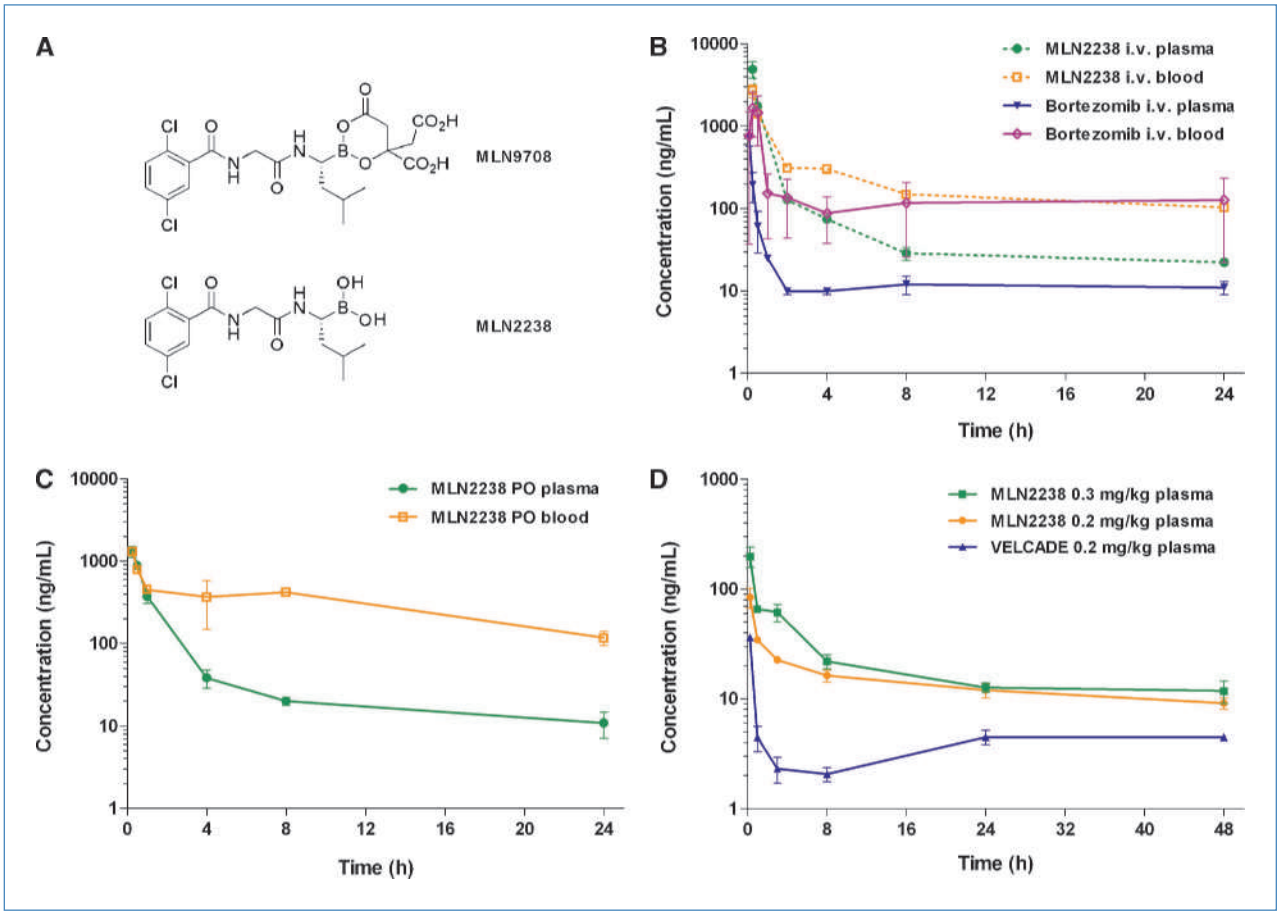

Figure 1. Structure of MLN9708. A, blood and plasma concentration versus time profile of MLN2238 and bortezomib in CB17-SCID mice following an acute i.v. administration (100 μL per mouse) at 14 or 0.8 mg/kg, respectively. B, blood and plasma concentration versus time profile following an acute oral administration of MLN2238 in CB17-SCID mice at 11 mg/kg (100 μL per mouse). C, plasma concentration versus time profile following an acute i.v. administration (200 μL per rat) of MLN2238 and bortezomib in nude rats at 0.3, 0.2, and 0.2 mg/kg, respectively. D, bars, SD. $n = 3$ for all time points, except 0.5 h after dose in plasma for MLN2238 i.v., 1 h after dose in plasma for bortezomib i.v., and 0.5 and 8 h after dose in blood for MLN2238 orally (PO), where $n = 2$.

Table 1. Summary of MLN2238 and bortezomib enzymology, pharmacokinetic, and pharmacodynamic parameters

	MLN2238	Bortezomib
Biochemical assays		
β5 K_i (nmol/L)	0.93 (0.64–1.4, n = 3)	0.55 (0.34–0.89, n = 3)
β5 IC_{50} (nmol/L)	3.4 (2.8–4.1, n = 3)	2.4 (2.0–2.9, n = 45)
β2 IC_{50} (nmol/L)	3,500	1,200
β1 IC_{50} (nmol/L)	31	24 (14.5–40, n = 12)
β5 dissociation half-life (min)	18 (6.8–30, n = 3)	110 (71–150, n = 3)
Cell-based assays		
MDA-MB-231 4×Ub-Luc EC_{50} (nmol/L)	525 (330–840, n = 4)	310 (230–400, n = 29)
E_{max} (fold stimulation)	265 (160–370, n = 4)	370 (330–410, n = 29)
HEK293 NF-κB-Luc EC_{50} (nmol/L)	55 (33–91, n = 7)	33 (27–40, n = 23)
E_{max} (% maximum inhibition)	99.3 (99.0–99.6, n = 7)	99.6 (99.3–100, n = 23)
Calu-6 Proteasome-Glo IC_{50} (nmol/L)	9.7 (n = 7)	4.8 (n = 12)
Calu-6 Proteasome-Glo (% activity),* t = 4 h, no washout	7.1 (3.6–10.6, n = 5)	3.45 (2.0–4.9, n = 5)
Calu-6 Proteasome-Glo (% Activity),* t = 4 h, washout	69 (66–71, n = 5)	20 (18–23, n = 5)
A375 ATPlite LD_{50} (nmol/L)	20	6.5
H460 ATPlite LD_{50} (nmol/L)	58	13
HCT-116 ATPlite LD_{50} (nmol/L)	19	4
HT-29 ATPlite LD_{50} (nmol/L)	52	7

Pharmacokinetic parameters

Agent	Dose and route	Matrix	C_{max} (ng/mL)	$AUC_{0–24h}$ (h·ng/mL)	Vd (L/kg)	F%
MLN2238	14 mg/kg i.v.	Plasma	17,000	8,090		
	14 mg/kg i.v.	Blood	10,500	9,660	20.2	
	11 mg/kg orally	Plasma	1,630	1,810		27.8
	11 mg/kg orally	Blood	1,710	6,310		59.5
Bortezomib	0.8 mg/kg i.v.	Plasma	321	485		
	0.8 mg/kg i.v.	Blood	548	4422	4.3	

Pharmacodynamic parameters

Agent	Dose and route	Matrix	E_{max} (I%)	$AUE_{0–24h}$ (%I·h)	AUE ratio (tumor/blood)
MLN2238	14 mg/kg i.v.	Blood	83.1†	718†	
	14 mg/kg i.v.	Tumor (CWR22)	69.1	1120	1.56
	14 mg/kg i.v.	Tumor (WSU-DLCL2)	77.0	1460	2.03
Bortezomib	0.8 mg/kg i.v.	Blood	88.3‡	1170‡	
	0.8 mg/kg i.v.	Tumor (CWR22)	44.8	804	0.69
	0.8 mg/kg i.v.	Tumor (WSU-DLCL2)	27.6	306	0.26

NOTE: Results are reported as mean (95% confidence interval, number of experiments).
Abbreviations: K_i, inhibition dissociation constant; E_{max}, maximum effect; F%, oral bioavailability; t = time; $AUC_{0–24\ h}$, AUC from 0 to 24 h; C_{max}, maximum concentration; Vd, volume of distribution; I%, percentage of inhibition.
*After exposure to 1 μmol/L MLN2238 or 1 μmol/L bortezomib for 30 min.
†For MLN2238, blood E_{max} = 81.3% to 85.0% (n = 2) and $AUE_{0–24h}$ = 554 to 882 (n = 2).
‡For bortezomib, blood E_{max} = 86.8% to 89.8% (n = 2) and $AUE_{0–24h}$ = 1,140 to 1,200 (n = 2).

The effect of MLN2238 or bortezomib on β5 activity was determined *in situ* using the Proteasome-Glo cell-based assay. The IC_{50} values determined by this assay following 1 hour of treatment with MLN2238 or bortezomib were in the low nanomolar range and comparable with those calculated with purified 20S proteasome. Recovery of proteasome activity was determined by performing washout experiments with MLN2238 or bortezomib. Cells were treated with the drug for 4 hours, after which the drug was removed and proteasome activity was assessed. Proteasome activity in MLN2238-treated cells recovered to 69% of control cells, whereas activity in bortezomib-treated

cells recovered to only 20% (Table 1). The difference in recovery of proteasome activity between MLN2238 and bortezomib is consistent with the observed differences in proteasome $t_{1/2}$ between the two molecules.

Cell viability studies were performed in a variety of mammalian cell lines to compare the *in vitro* antiproliferative effects of MLN2238 with bortezomib. Studies performed with A375 (lung), H460 (lung), HCT-116 (colon), and HT-29 (colon) cells revealed similar LD_{50} values for the two compounds, which ranged from 4 to 58 nmol/L (Table 1).

Taken together, these *in vitro* studies show that MLN2238 is a potent inhibitor of the β5 site of the 20S proteasome and that MLN2238 dissociated more rapidly from the proteasome than bortezomib, consistent with faster recovery of proteasome activity observed in the Proteasome-Glo assay. Given the high concentrations of proteasome found in RBCs, we hypothesized that RBC partitioning would serve as a drug sink for bortezomib and limit its distribution outside of the blood compartment; the shorter proteasome $t_{1/2}$ of MLN2238 should allow improved drug distribution into tissues. To address this issue directly, a series of pharmacokinetic, pharmacodynamic, and efficacy studies with MLN2238 and bortezomib were performed in different xenograft models.

Pharmacokinetics of MLN2238 and bortezomib. To determine the pharmacokinetic profile of MLN2238 and bortezomib, mice were administered a single dose of MLN2238 at 14 mg/kg i.v. and 11 mg/kg orally or bortezomib at 0.8 mg/kg i.v. These doses represent the maximum tolerated dose (MTD) for each drug for the specified route of administration. Exposures were determined by measuring the blood and plasma drug concentrations at various time points following the initial dose (Table 1). The concentration-versus-time curve of i.v. administered MLN2238 displayed a distinct biexponential profile with a steep ini-

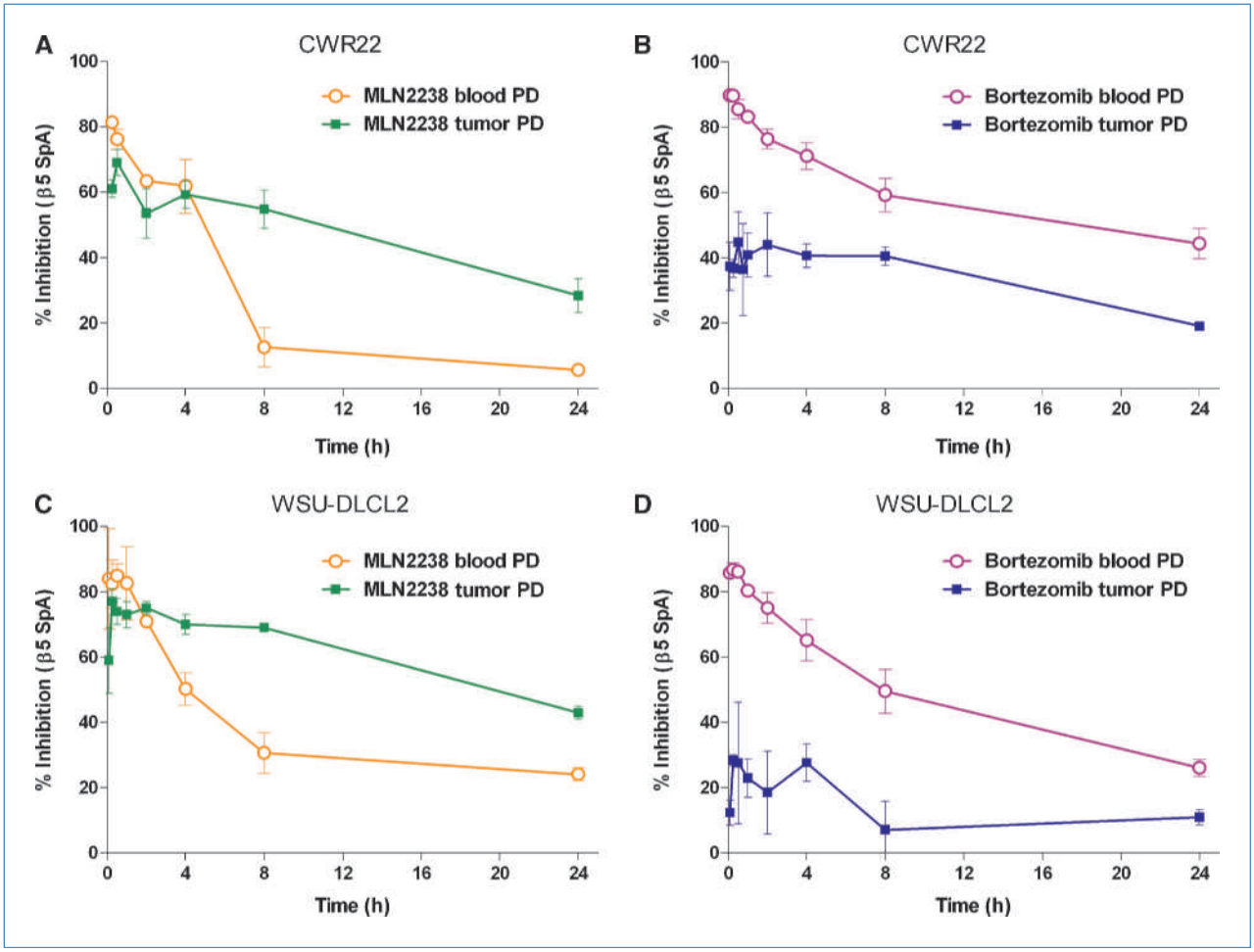

Figure 2. Blood and tumor proteasome inhibition versus time profile of MLN2238 (14 mg/kg; A and C) and bortezomib (0.8 mg/kg; B and D) following acute i.v. administration in CWR22 (A and B) and WSU-DLCL2 (C and D) tumor-bearing mice. Pharmacodynamic responses in blood and tumor were determined by measuring 20S proteasome β5 enzyme inhibition in blood and tumor at different time points.

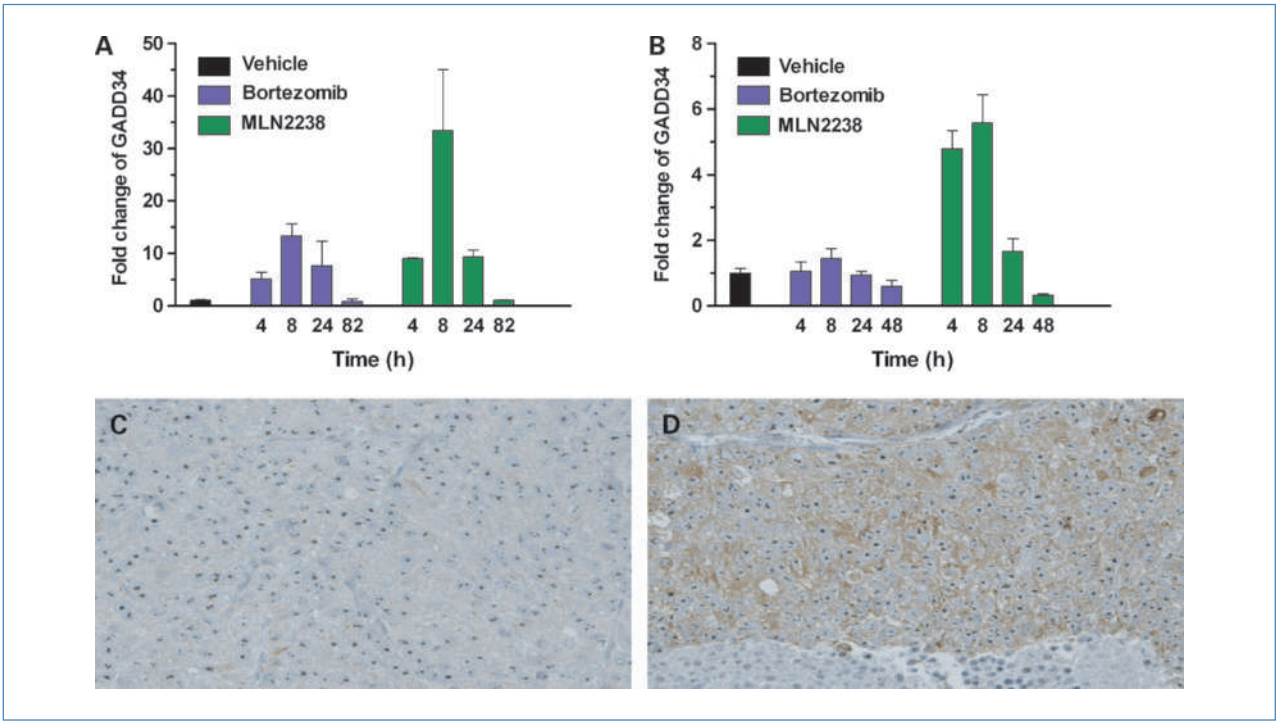

Figure 3. Pharmacodynamic responses in tumor were determined by measuring GADD34 protein levels at different time points via Western blot and quantitated with the Odyssey Infrared Imaging System. A and B, normalized GADD34 response versus time profile shown as fold change from vehicle control following acute i.v. administration of MLN2238 at 10 mg/kg and bortezomib at 0.8 mg/kg in CWR22 (A) and WSU-DLCL2 (B) tumor-bearing mice. Columns, mean of three tumors per group, except CWR22 vehicle group with four tumors and WSU-DLCL2 vehicle group with five tumors; bars, SD. Immunohistochemical staining (C and D) for GADD34 in CWR22 xenograft tumors 8 h following an acute i.v. dose of either vehicle (C) or MLN2238 at 14 mg/kg (D).

tial distribution phase and a long terminal $t_{1/2}$ (>24 hours; Fig. 1B). Due to extensive RBC partitioning, whole-body tissue distribution is most accurately reflected in blood volume distribution at steady state ($Vd_{ss,\ b}$) rather than plasma volume distribution at steady state ($Vd_{ss,\ p}$). MLN2238 showed larger $Vd_{ss,\ b}$ (20.2 L/kg) compared with bortezomib (4.3 L/kg), providing supportive evidence that MLN2238 more easily moves from the blood compartment

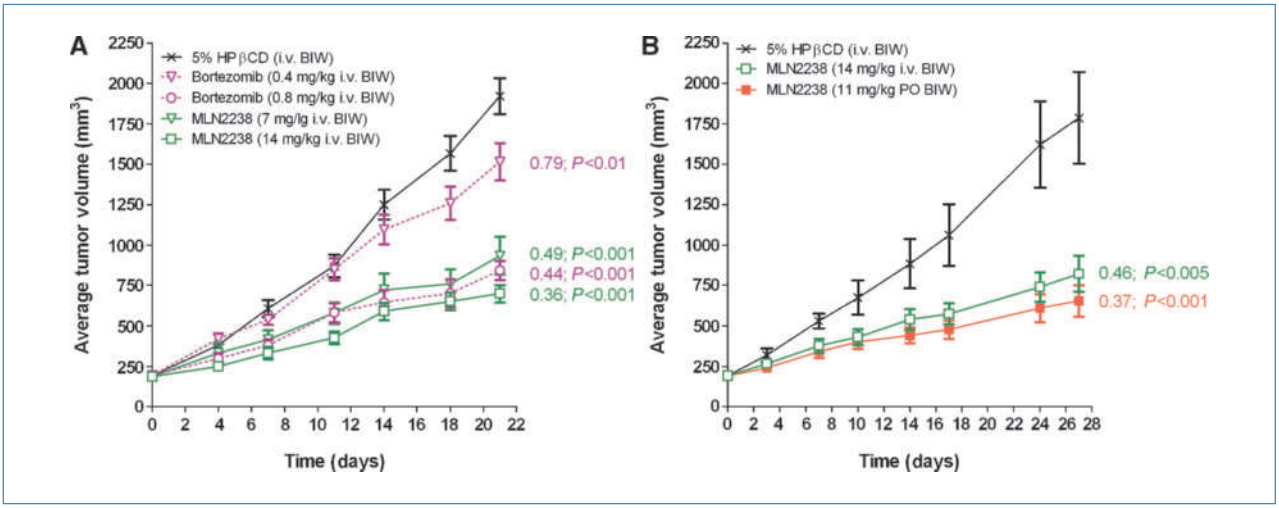

Figure 4. Antitumor activity of MLN2238 and bortezomib in CWR22 tumor-bearing mice (n = 10). A, animals were dosed i.v. twice weekly (BIW) with vehicle (5% HPβCD), bortezomib (0.4 and 0.8 mg/kg in 0.9% saline), and MLN2238 (7 and 14 mg/kg in 5% HPβCD). B, animals were dosed i.v. twice weekly with vehicle, i.v. twice weekly with MLN2238 (14 mg/kg), or orally twice weekly with MLN2238 (11 mg/kg). Points, average tumor volume in each treatment group; bars, SE. T/C and P values were calculated as described in Materials and Methods. A P value of ≤0.05 was considered significant.

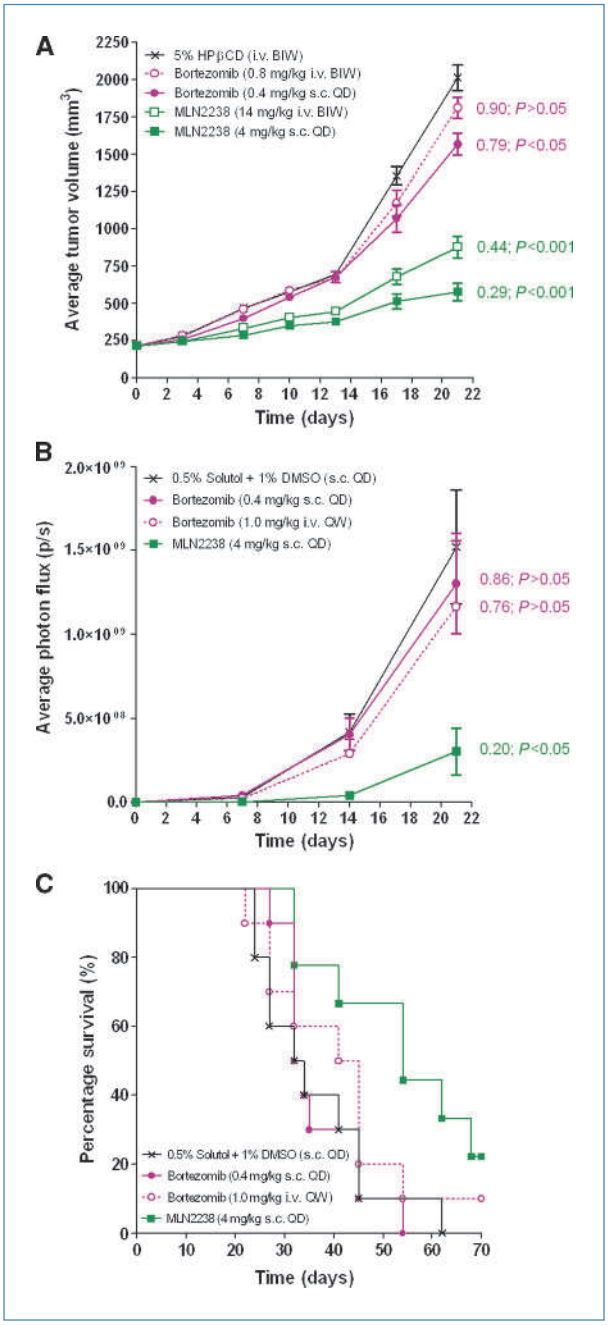

Figure 5. Antitumor activity of MLN2238 and bortezomib in two lymphoma xenograft models. Each treatment group consisted of 10 mice. A, antitumor activity in WSU-DLCL2 xenografts. Animals were dosed with vehicle (5% HPβCD i.v. twice weekly), bortezomib (0.8 mg/kg i.v. twice weekly or 0.4 mg/kg s.c. QD), or MLN2238 (14 mg/kg i.v. twice weekly or 4 mg/kg s.c. QD) for 3 consecutive weeks. B, antitumor activity in the OCI-Ly7-Luc disseminated lymphoma model. Animals were dosed with vehicle (0.5% Solutol + 1% DMSO s.c. QD), bortezomib (0.4 mg/kg in 0.9% saline s.c. QD), bortezomib (1.0 mg/kg in 0.9% saline i.v. QW), or MLN2238 (4 mg/kg in 0.5% Solutol + 1% DMSO s.c. QD) for 3 consecutive weeks. Points, average tumor volume; bars, SE. T/C and *P* values were calculated as described in Materials and Methods. A *P* value of ≤0.05 was considered significant. C, Kaplan-Meier survival profile.

into the tissue compartment. MLN2238 also showed moderate oral bioavailability (Table 1; Fig. 1C). To determine the pharmacokinetic profile of MLN2238 and bortezomib in a second species, Sprague-Dawley rats were administered a single i.v. dose of MLN2238 at either 0.3 or 0.2 mg/kg or bortezomib at 0.2 mg/kg. Both MLN2238 doses provided a greater plasma exposure (AUC_{0-48h} of 704 and 1,070 h·ng/mL for 0.2 and 0.3 mg/kg doses, respectively) compared with bortezomib (AUC_{0-48h} of 206 h·ng/mL), confirming that MLN2238 also has improved plasma exposure compared with bortezomib in rodents (Fig. 1D).

MLN2238 induces a greater pharmacodynamic response than bortezomib in xenograft tumors. To further evaluate the activity of MLN2238 *in vivo*, a series of pharmacodynamic studies were performed in CB17-SCID mice bearing human prostate (CWR22) or human lymphoma tumors (WSU-DLCL2). Pharmacodynamic responses were assessed by measuring (*a*) the degree of 20S proteasome inhibition and (*b*) the expression levels of the GADD34 protein.

Blood and tumor 20S proteasome inhibition versus time profiles were generated for MLN2238 and bortezomib from both CWR22 and WSU-DLCL2 xenografts (Fig. 2). The AUE was calculated from 0 to 24 hours (AUE_{0-24h}) for both blood and tumor (Table 1). These AUEs represent the summation of the pharmacodynamic effect over a defined period of time in a particular tissue compartment. Calculating the tumor to blood AUE ratio provided a functional reflection of the distribution and durable pharmacodynamic effect of the drug in different tissue compartments. The maximum level of blood proteasome inhibition (E_{max}) following an acute i.v. dose of either MLN2238 (83.1%) or bortezomib (88.3%) was nearly identical (Table 1). However, the duration of the effect differed between the two molecules, with bortezomib having a more sustained response and, therefore, a greater blood AUE than MLN2238 (Fig. 2B and D). In contrast to blood, MLN2238 showed both greater maximum and sustained tumor proteasome inhibition compared with bortezomib in both xenograft models (Table 1; Fig. 2A and C). The tumor to blood AUE ratio for MLN2238 in CWR22s and WSU-DLCL2s was 1.56 and 2.03, respectively, compared with 0.69 and 0.26 for bortezomib (Table 1). Consistent with the pharmacokinetic profiles described for these two molecules (i.e., MLN2238 has a greater $Vd_{ss,\ b}$), these results showed that MLN2238 had a greater pharmacodynamic effect in tumor compared with blood, whereas the opposite was true for bortezomib. Consistent with the improved tumor E_{max} in MLN2238-treated mice, these data confirm that MLN2238 had a greater overall tumor pharmacodynamic effect than bortezomib as assessed by 20S inhibition.

Additional pharmacodynamic markers were examined to study the downstream effects of proteasome inhibition. One of the consequences of proteasome inhibition is the accumulation of proteins associated with the endoplasmic reticulum (ER) stress pathway and the unfolded protein response (UPR) pathway (11, 45–50). One of these proteins is GADD34, a stress-inducible gene that is also upregulated in response to DNA damage, hypoxia, and energy depletion

(51). Western blot analyses were performed on tumors isolated from CWR22 and WSU-DLCL2 xenograft-bearing mice treated with either MLN2238 or bortezomib (Fig. 3). Increased GADD34 expression was seen in CWR22 xenograft tumors following MLN2238 or bortezomib treatment, whereas an even greater response was seen following MLN2238 treatment (Fig. 3A). Similarly, bortezomib treatment only led to a minor increase in GADD34 levels in WSU-DLCL2 xenograft tumors, whereas MLN2238 strongly induced its expression (Fig. 3B). To confirm these results, and to get a better understanding of the magnitude of response across individual cells within the tumor, immunohistochemical staining was performed using the anti-GADD34 antibody (Proteintech). Strong GADD34 staining, reflecting increases in GADD34 protein levels, was seen across the majority of tumor cells in CWR22 xenografts 8 hours after a single i.v. dose of MLN2238 at 14 mg/kg (Fig. 3D) compared with very low staining in vehicle-treated CWR22 xenografts (Fig. 3C). Approximately a 5-fold increase in the total number of GADD34-positive cells was seen at 8 and 24 hours following MLN2238 treatment compared with vehicle control–treated tumors (Supplementary Fig. S1). In WSU-DLCL2 xenograft tumors, bortezomib treatment led to only a minor increase in GADD34 levels measured by Western blot, whereas MLN2238 strongly induced its expression (Fig. 3B). In addition, examining levels of ATF3, another gene upregulated during ER stress and UPR activation (48, 52, 53), revealed a similar pattern, with a greater number of cells staining positively for ATF3 following treatment of WSU-DLCL2 xenograft tumors with MLN2238 compared with bortezomib (Supplementary Fig. S2). These results confirm that the improved tumor exposure seen with MLN2238 translated into an improved tumor pharmacodynamic response both at the level of and downstream from the proteasome.

MLN2238 shows antitumor activity in the CWR22 xenograft model. To confirm that the pharmacodynamic responses seen in CWR22 xenografts would translate into antitumor activity, a series of efficacy experiments were performed comparing MLN2238 with bortezomib.

The antitumor effects of MLN2238 dosed at 14 mg/kg i.v. or 7 mg/kg i.v. were compared with bortezomib dosed at 0.8 mg/kg i.v. or 0.4 mg/kg i.v. on a twice weekly regimen (Fig. 4A). The high dose for both MLN2238 and bortezomib showed similar antitumor activity in this model (T/C = 0.36 and 0.44, respectively). However, MLN2238 (7 mg/kg) showed greater efficacy at a 0.5 MTD dose compared with a 0.5 MTD dose of bortezomib (0.4 mg/kg; T/C = 0.49 compared with T/C = 0.79, respectively; Fig. 4A).

MLN2238 has moderate orally bioavailability (Table 1). In Fig. 4B, we show that oral dosing of MLN2238 resulted in antitumor activity in the CWR22 xenograft model (T/C = 0.37). Taken together, these results show that the human prostate CWR22 model is responsive to proteasome inhibition. Furthermore, a direct comparison between MLN2238 and bortezomib revealed similar antitumor activity when dosed at their respective MTDs; however, when both compounds were dosed at their respective 0.5 MTDs, MLN2238 showed improved activity over bortezomib (Fig. 4A).

MLN2238 shows improved efficacy compared with bortezomib in two models of lymphoma. MLN2238 showed greater tumor pharmacodynamic responses in WSU-DLCL2 xenografts compared with bortezomib (Table 1; Figs. 2 and 3). To assess whether the more robust pharmacodynamic response translated to greater antitumor activity, an efficacy study was performed in WSU-DLCL2 tumor-bearing mice. The antitumor effects of MLN2238 [dosed at 14 mg/kg i.v. twice weekly or 4 mg/kg s.c. once daily (QD)] were directly compared with bortezomib (dosed at 0.8 mg/kg i.v. twice weekly or 0.4 mg/kg s.c. QD; Fig. 5A). In this experiment, neither of the bortezomib doses showed strong antitumor activity (T/C = 0.79 and 0.9 for 0.8 mg/kg i.v. and 0.4 mg/kg s.c., respectively). In contrast, both intermittent and continuous MLN2238 dosing regimens showed strong antitumor activity (T/C = 0.44 and 0.29 for 14 mg/kg i.v. and 4 mg/kg s.c., respectively) and generated a greater apoptotic response in tumor tissue as measured by levels of cleaved caspase-3 (Supplementary Fig. S3).

The antitumor activity of MLN2238 and bortezomib was evaluated in a disseminated model of lymphoma. The ability of both drugs to reduce tumor burden and improve overall survival was assessed in this systemic lymphoma model. NOD-SCID mice were inoculated with OCI-Ly7-Luc cells expressing a luciferase reporter gene. Bioluminescent scans, obtained via quantitative Xenogen imaging, allowed tumor growth to be tracked over time in live animals. The strongest antitumor response was seen following treatment with MLN2238 at 4.0 mg/kg s.c. QD (T/C = 0.20; Fig. 5B). This dosing regimen also significantly prolonged overall survival in this model compared with vehicle-treated controls (median survival was 54 versus 33 days, $P = 0.05$; Fig. 5C). Much weaker antitumor responses were seen following bortezomib treatment at 0.4 mg/kg s.c. QD or 1.0 mg/kg i.v. once weekly (T/C = 0.86 and 0.76, respectively). These bortezomib dosing regimens also did not significantly prolong survival (median survival was 33 and 43 days, respectively; $P > 0.99$ for both; Fig. 5C).

In summary, we have identified a second-generation small-molecule inhibitor of the proteasome. It has different physicochemical properties compared with bortezomib, including a shorter proteasome dissociation $t_{1/2}$, which we believe plays a critical role in the ability of this molecule to distribute into tissues. Improved pharmacokinetic and tolerability allow this molecule to be administered at higher doses, resulting in greater blood and plasma exposures. Consistent with these findings, we found a greater pharmacodynamic response in multiple xenograft models treated with MLN2238 compared with bortezomib, particularly in tumor, supporting our hypothesis that MLN2238 has improved distribution characteristics. Superior bioavailability also allows this molecule to be dosed orally, whereas bortezomib is restricted to i.v. and s.c. dosing regimens to achieve acceptable exposure levels. Data generated from both s.c. and disseminated xenograft efficacy studies show that MLN2238 has greater antitumor activity when administered by either intermittent or continuous dosing regimens and improves overall survival compared with bortezomib. Taken together, these data support the clinical

development of MLN9708 for both hematologic and solid tumor indications.

Disclosure of Potential Conflicts of Interest

No potential conflicts of interest were disclosed.

Acknowledgments

The costs of publication of this article were defrayed in part by the payment of page charges. This article must therefore be hereby marked *advertisement* in accordance with 18 U.S.C. Section 1734 solely to indicate this fact.

Received 07/24/2009; revised 12/14/2009; accepted 12/15/2009; published OnlineFirst 02/16/2010.

References

1. Orlowski RZ, Kuhn DJ. Proteasome inhibitors in cancer therapy: lessons from the first decade. Clin Cancer Res 2008;14:1649–57.
2. Dalton WS. The proteasome. Semin Oncol 2004;31:3–9; discussion 33.
3. Delic J, Masdehors P, Omura S, et al. The proteasome inhibitor lactacystin induces apoptosis and sensitizes chemo- and radioresistant human chronic lymphocytic leukaemia lymphocytes to TNF-α-initiated apoptosis [see comment]. Br J Cancer 1998;77:1103–7.
4. LeBlanc R, Catley LP, Hideshima T, et al. Proteasome inhibitor PS-341 inhibits human myeloma cell growth *in vivo* and prolongs survival in a murine model. Cancer Res 2002;62:4996–5000.
5. Orlowski RZ, Eswara JR, Lafond-Walker A, et al. Tumor growth inhibition induced in a murine model of human Burkitt's lymphoma by a proteasome inhibitor. Cancer Res 1998;58:4342–8.
6. Shinohara K, Tomioka M, Nakano H, et al. Apoptosis induction resulting from proteasome inhibition. Biochem J 1996;317:385–8.
7. Adams J. Proteasome inhibitors as new anticancer drugs. Curr Opin Oncol 2002;14:628–34.
8. Adams J. Potential for proteasome inhibition in the treatment of cancer. Drug Discov Today 2003;8:307–15.
9. Adams J. The development of proteasome inhibitors as anticancer drugs. Cancer Cell 2004;5:417–21.
10. Nalepa G, Rolfe M, Harper JW. Drug discovery in the ubiquitin-proteasome system. Nat Rev 2006;5:596–613.
11. Nencioni A, Grunebach F, Patrone F, Ballestrero A, Brossart P. Proteasome inhibitors: antitumor effects and beyond. Leukemia 2007;21:30–6.
12. Voorhees PM, Dees EC, O'Neil B, Orlowski RZ. The proteasome as a target for cancer therapy. Clin Cancer Res 2003;9:6316–25.
13. Belch A, Kouroukis CT, Crump M, et al. A phase II study of bortezomib in mantle cell lymphoma: the National Cancer Institute of Canada Clinical Trials Group trial IND.150. Ann Oncol 2007;18:116–21.
14. Fisher RI, Bernstein SH, Kahl BS, et al. Multicenter phase II study of bortezomib in patients with relapsed or refractory mantle cell lymphoma. J Clin Oncol 2006;24:4867–74.
15. Goy A, Younes A, McLaughlin P, et al. Phase II study of proteasome inhibitor bortezomib in relapsed or refractory B-cell non-Hodgkin's lymphoma. J Clin Oncol 2005;23:667–75.
16. O'Connor OA, Wright J, Moskowitz C, et al. Phase II clinical experience with the novel proteasome inhibitor bortezomib in patients with indolent non-Hodgkin's lymphoma and mantle cell lymphoma. J Clin Oncol 2005;23:676–84.
17. Orlowski RZ, Stinchcombe TE, Mitchell BS, et al. Phase I trial of the proteasome inhibitor PS-341 in patients with refractory hematologic malignancies. J Clin Oncol 2002;20:4420–7.
18. Richardson PG, Barlogie B, Berenson J, et al. A phase 2 study of bortezomib in relapsed, refractory myeloma. N Engl J Med 2003;348:2609–17.
19. Richardson PG, Barlogie B, Berenson J, et al. Extended follow-up of a phase II trial in relapsed, refractory multiple myeloma: final time-to-event results from the SUMMIT trial. Cancer 2006;106:1316–9.
20. Richardson PG, Sonneveld P, Schuster M, et al. Extended follow-up of a phase 3 trial in relapsed multiple myeloma: final time-to-event results of the APEX trial. Blood 2007;110:3557–60.
21. Richardson PG, Sonneveld P, Schuster MW, et al. Bortezomib or high-dose dexamethasone for relapsed multiple myeloma. N Engl J Med 2005;352:2487–98.
22. Chauhan D, Singh A, Brahmandam M, et al. Combination of proteasome inhibitors bortezomib and NPI-0052 trigger *in vivo* synergistic cytotoxicity in multiple myeloma. Blood 2008;111:1654–64.
23. Cusack JC, Jr., Liu R, Xia L, et al. NPI-0052 enhances tumoricidal response to conventional cancer therapy in a colon cancer model. Clin Cancer Res 2006;12:6758–64.
24. Demo SD, Kirk CJ, Aujay MA, et al. Antitumor activity of PR-171, a novel irreversible inhibitor of the proteasome. Cancer Res 2007;67:6383–91.
25. Dorsey BD, Iqbal M, Chatterjee S, et al. Discovery of a potent, selective, and orally active proteasome inhibitor for the treatment of cancer. J Med Chem 2008;51:1068–72.
26. Mitsiades CS, Hayden PJ, Anderson KC, Richardson PG. From the bench to the bedside: emerging new treatments in multiple myeloma. Best Pract Res 2007;20:797–816.
27. Piva R, Ruggeri B, Williams M, et al. CEP-18770: a novel, orally active proteasome inhibitor with a tumor-selective pharmacologic profile competitive with bortezomib. Blood 2008;111:2765–75.
28. Sterz J, von Metzler I, Hahne JC, et al. The potential of proteasome inhibitors in cancer therapy. Expert Opin Investig Drugs 2008;17:879–95.
29. Kuhn DJ, Chen Q, Voorhees PM, et al. Potent activity of carfilzomib, a novel, irreversible inhibitor of the ubiquitin-proteasome pathway, against preclinical models of multiple myeloma. Blood 2007;110:3281–90.
30. Stapnes C, Doskeland AP, Hatfield K, et al. The proteasome inhibitors bortezomib and PR-171 have antiproliferative and proapoptotic effects on primary human acute myeloid leukaemia cells. Br J Haematol 2007;136:814–28.
31. Arendt CS, Hochstrasser M. Identification of the yeast 20S proteasome catalytic centers and subunit interactions required for active-site formation. Proc Natl Acad Sci U S A 1997;94:7156–61.
32. Baumeister W, Walz J, Zuhl F, Seemuller E. The proteasome: paradigm of a self-compartmentalizing protease. Cell 1998;92:367–80.
33. Coux O, Tanaka K, Goldberg AL. Structure and functions of the 20S and 26S proteasomes. Annu Rev Biochem 1996;65:801–47.
34. Heinemeyer W, Ramos PC, Dohmen RJ. The ultimate nanoscale mincer: assembly, structure and active sites of the 20S proteasome core. Cell Mol Life Sci 2004;61:1562–78.
35. Adams J, Behnke M, Chen S, et al. Potent and selective inhibitors of the proteasome: dipeptidyl boronic acids. Bioorg Med Chem Lett 1998;8:333–8.
36. Williamson MJ, Blank JL, Bruzzese FJ, et al. Comparison of biochemical and biological effects of ML858 (salinosporamide A) and bortezomib. Mol Cancer Ther 2006;5:3052–61.
37. Lightcap ES, McCormack TA, Pien CS, Chau V, Adams J, Elliott PJ. Proteasome inhibition measurements: clinical application. Clin Chem 2000;46:673–83.
38. Elliott PJ, Soucy TA, Pien CS, Adams J, Lightcap ES. Assays for proteasome inhibition. Methods Mol Med 2003;85:163–72.
39. Kumatori A, Tanaka K, Inamura N, et al. Abnormally high expression of proteasomes in human leukemic cells. Proc Natl Acad Sci U S A 1990;87:7071–5.
40. Li X, Amazit L, Long W, Lonard DM, Monaco JJ, O'Malley BW. Ubiquitin- and ATP-independent proteolytic turnover of p21 by the REGγ-proteasome pathway. Mol Cell 2007;26:831–42.
41. Tambyrajah WS, Bowler LD, Medina-Palazon C, Sinclair AJ. Cell cycle-dependent caspase-like activity that cleaves p27(KIP1) is the β(1) subunit of the 20S proteasome. Arch Biochem Biophys 2007;466:186–93.
42. Touitou R, Richardson J, Bose S, Nakanishi M, Rivett J, Allday MJ. A degradation signal located in the C-terminus of p21WAF1/CIP1 is a binding site for the C8 α-subunit of the 20S proteasome. EMBO J 2001;20:2367–75.

43. Ang XL, Harper JW. Interwoven ubiquitination oscillators and control of cell cycle transitions. Sci STKE 2004;2004:pe31.
44. Karin M, Lin A. NF-κB at the crossroads of life and death. Nat Immunol 2002;3:221–7.
45. Lee AH, Iwakoshi NN, Anderson KC, Glimcher LH. Proteasome inhibitors disrupt the unfolded protein response in myeloma cells. Proc Natl Acad Sci U S A 2003;100:9946–51.
46. Fribley A, Zeng Q, Wang CY. Proteasome inhibitor PS-341 induces apoptosis through induction of endoplasmic reticulum stress-reactive oxygen species in head and neck squamous cell carcinoma cells. Mol Cell Biol 2004;24:9695–704.
47. Kraus M, Malenke E, Gogel J, et al. Ritonavir induces endoplasmic reticulum stress and sensitizes sarcoma cells toward bortezomib-induced apoptosis. Mol Cancer Ther 2008;7:1940–8.
48. Wang Q, Mora-Jensen H, Weniger MA, et al. ERAD inhibitors integrate ER stress with an epigenetic mechanism to activate BH3-only protein NOXA in cancer cells. Proc Natl Acad Sci U S A 2009;106:2200–5.
49. Meister S, Schubert U, Neubert K, et al. Extensive immunoglobulin production sensitizes myeloma cells for proteasome inhibition. Cancer Res 2007;67:1783–92.
50. Obeng EA, Carlson LM, Gutman DM, Harrington WJ, Jr., Lee KP, Boise LH. Proteasome inhibitors induce a terminal unfolded protein response in multiple myeloma cells. Blood 2006;107:4907–16.
51. Hollander MC, Zhan Q, Bae I, Fornace AJ, Jr. Mammalian GADD34, an apoptosis- and DNA damage-inducible gene. J Biol Chem 1997;272:13731–7.
52. Hai T, Wolfgang CD, Marsee DK, Allen AE, Sivaprasad U. ATF3 and stress responses. Gene Expr 1999;7:321–35.
53. Jiang HY, Wek SA, McGrath BC, et al. Activating transcription factor 3 is integral to the eukaryotic initiation factor 2 kinase stress response. Mol Cell Biol 2004;24:1365–77.